

Article

2D/3D Perovskite Engineering Eliminates Interfacial Recombination Losses in Hybrid Perovskite Solar Cells

Albertus A. Sutanto¹, Pietro Caprioglio^{2,3}, Nikita Drigo¹, Yvonne J. Hofstetter⁴, Ines Garcia-Benito¹, Valentin I. E. Queloz¹, Dieter Neher², Mohammad Khaja Nazeeruddin^{1,*}, Martin Stolterfoht^{2,**}, Yana Vaynzof^{4,***}, Giulia Grancini^{1,5,6,****}

¹Group for Molecular Engineering of Functional Materials, Institute of Chemical Sciences and Engineering, EPFL Valais Wallis, Rue de l'Industrie 17, CH-1951 Sion, Switzerland.

²University of Potsdam, Institut für Physik und Astronomie, Potsdam, Germany

³Young Investigator Group Perovskite Tandem Solar Cells, Helmholtz-Zentrum Berlin für Materialien und Energie GmbH, 12489 Berlin, Germany

⁴Dresden Integrated Center for Applied Physics and Photonic Materials (IAPP) und Centre for Advancing Electronics Dresden (cfaed), Technical University of Dresden, 01062 Dresden

⁵Department of Chemistry and INSTM, University of Pavia, Via T. Taramelli 14, 27100 Pavia, Italy

⁶Lead contact

*Correspondence: mdkhaja.nazeeruddin@epfl.ch

**Correspondence: stolterf@uni-potsdam.de

***Correspondence: yana.vaynzof@tu-dresden.de

****Correspondence: giulia.grancini@unipv.it

SUMMARY

Interface Engineering and design is paramount in the optimization of multilayer device stack. This stem true for multi-dimensional (2D/3D) perovskite based solar cells, where high efficiency can be combined with promising device durability. However, the ultimate complex function of 2D/3D device interface remains vague. Here, we provide the exact knowledge on the interface energetics and we demonstrate that the 2D/3D perovskite interface forms a *p-n* junction able of reducing the electron density at the hole transport layer interface and ultimately suppressing interfacial recombination. As a consequence, we demonstrate photovoltaic devices with enhanced fill factor (FF) and open-circuit voltage (V_{oc}) of 1.19V which approaches the potential internal Quasi-Fermi Level Splitting (QFLS) voltage of the perovskite absorber, nullifying the interfacial losses. We thus identify the essential parameters and energetic alignment scenario required for 2D/3D perovskite systems in order to surpass the current limitations of hybrid perovskite solar cell performances.

Keywords: perovskite solar cells, 2D perovskite, interface, recombination, UPS, *p-n* junction, quasi-fermi level splitting.

INTRODUCTION

Understanding and exploiting interfacial physics is key in perovskite solar cell engineering and optimization.^{1, 2} That is especially true when interface losses play a dominant role and complex interface functionalization is essential to minimize them. In the field of hybrid perovskite engineering, much attention has been lately focused on multi-dimensional perovskite interfaces consisting of a wider band gap layered (namely, two dimensional-2D) perovskite deposited between the bulk 3D perovskite and the hole transporting layer (HTL) in a standard mesoporous configuration.³⁻⁹ Such configuration is currently among the most effective strategies to enhance both the efficiency and stability of perovskite solar cells.^{3, 10-14}

It is generally considered that the 2D perovskite acts as both an efficient mean to passivate the surface traps (leading to reduced defect recombination) and an electron blocking layer due to its wider band gap.¹⁵⁻²⁰ However, despite these empirical observations, the energetic alignment at the interface and the relative function of the 2D/3D interface is only qualitatively depicted with a only a partial understanding of these aspects. This lack of knowledge prevents the advancement of device efficiencies towards the theoretical Shockley-Queisser predictions beyond the common trial and error approach.²¹ More specifically, the exact role of the interface band structure and energetics and their effect on the processes and loss mechanisms remains largely unexplored, mainly due to the lack of direct experimental evidences.

In this work we target the interface energetics of optimized 2D/3D perovskite systems by measuring the vertical energy level landscape by an innovative UPS depth profiling technique. The analysis reveals intriguing variations of the interfacial energetics which depend on the chemical nature of 2D overlayer. Specifically, we explore a series of thiophene based cations that form the 2D perovskite layer, which differ slightly in their chemical structure, and which when integrated in a 2D/3D based perovskite solar cell, deliver approximately 21% power conversion efficiency and open-circuit voltage (V_{oc}) approaching 1.2 V. The photovoltaic performance is intimately linked to 2D/3D interfacial band bending and a natural formation of a *p-n* junction in optimal devices.

By calculating the quasi-Fermi level splitting (QFLS) from photoluminescence quantum yield (PLQY) for the neat material and the complete device, we identify that the optimal energetic alignment and reduced electron density at the interface serve as the reasons for such a

The bigger picture

Understanding interface energetics and physics is paramount for an exact knowledge on the device function and operation. This stem true for solar cells and for devices where interfaces are crucial. In this work, we determine for the first time the exact knowledge on the interface energetics across 2D/3D perovskite interfaces showing that it forms a *p-n* junction able of suppressing the interfacial recombination losses. This led to the photovoltaic devices with high open-circuit voltage which approaches the potential internal Quasi-Fermi Level Splitting of the perovskite absorber, nullifying the losses, a breakthrough for the field.

significant reduction in the non-radiative interfacial recombination losses. This allows us to reach radiative efficiencies of 2% in completed devices which is far above average.² Importantly, the recombination mechanisms proposed is corroborated by drift-diffusion simulation. The optimized 2D/3D interface shows zero interfacial voltage losses, reaching the QFLS-potential of the neat perovskite absorber and thus nullifying the energy losses at the interfaces. As such, we rationalized the mechanisms and the effect of 2D/3D interfaces on the effective reduction of the interfacial energy losses, providing a clear path for pushing perovskite solar cells performances closer to their theoretical limits.²

Here, we elucidate fundamental principles of how the creation of 3D/2D heterojunctions and the energy alignment at the hole-selective interface allows to overcome the decisive interfacial recombination losses of minority carriers at the interface to spiro-OMeTAD interface. This is achieved with a 2-TMAI 2D perovskite layer which forms an apparent *p-n* junction with the perovskite, thereby blocking the minority carriers from reaching the spiro-OMeTAD layer. Notably, in this system, the main voltage loss is only due to non-radiative recombination in the perovskite absorber layer, while interface recombination is essentially absent. This finding bares important implications for further perovskite design as several perovskites now achieve radiative efficiencies that are very close to the radiative limits.^{2, 22-25} Hence, our approach to effectively suppress the interfacial recombination may hold the key to create near ideal perovskite cells in the near future if applied to perovskite layers with very high PLQYs.

RESULTS AND DISCUSSION

The 2D/3D interfaces investigated here are based on a novel set of bulky thiophene-terminated cations, namely 2-thiophenemethylammonium iodide (2-TMAI),^{9, 26} 2-thiophenemethylammonium bromide (2-TMABr), and 2-thiophenemethylammonium chloride (2-TMACl) that serve as a building block for the formation of the 2D perovskite layer on top of 3D bulk layer (Figure 1a). The 3D perovskite layer is based on a triple-cation composition [(FAPbI₃)_{0.87}(MAPbBr₃)_{0.13}]_{0.92}(CsPbI₃)_{0.08} with a bandgap of 1.610 eV. The chemical structures of the thiophene-methylammonium salts are shown in Figure 1b. The three different 2-thiophenemethylammonium halides (2-TMAX, where X: Cl, Br, I) were prepared from the commercially available amines and the corresponding acids (see experimental methods). The salts were then diluted in isopropanol (IPA) and dynamically spin-coated on top of the triple-cation based 3D perovskite film. 2D perovskites are selectively grown by controlling the excess PbI₂ composition (PbI₂:FAI = 1.05:1) in the 3D perovskite which reacts with the thiophene ammonium halide cations to form the 2D layer.^{4, 9, 26}

Figure 1b shows also the X-ray diffraction (XRD) patterns of the 2D/3D films collected at a low diffraction angle. When the 2-TMAX is used to coat the 3D layer, intense reflexes at 4.3° and 8.6° appear at the XRD diffractograms, consistent with the key characteristic peaks of 2D perovskites (*n*=2).^{9, 26} In case of 2-TMAI, an additional reflection at 6.1° was observed which corresponds to the *n*=1 phase of 2D perovskite.⁹ The XRD pattern of 3D perovskite layer as the control are reported on Figure S1. Cross-sectional scanning electron microscopy (SEM) images shown in Figure 1c show that the 500 nm thick 3D perovskite layer is continuously coated by a 2D overlayer with a thickness of approximately 50-60 nm. The top surface images reveal that the formation of the 2D layers results in smoother surfaces, with less defined grain boundaries and crystals borders. This is particularly evident for the cases of 2-TMAI and 2-TMABr, while for the case of 2-TMACl a distribution of distinct phases with larger and more elongated grains is visible.

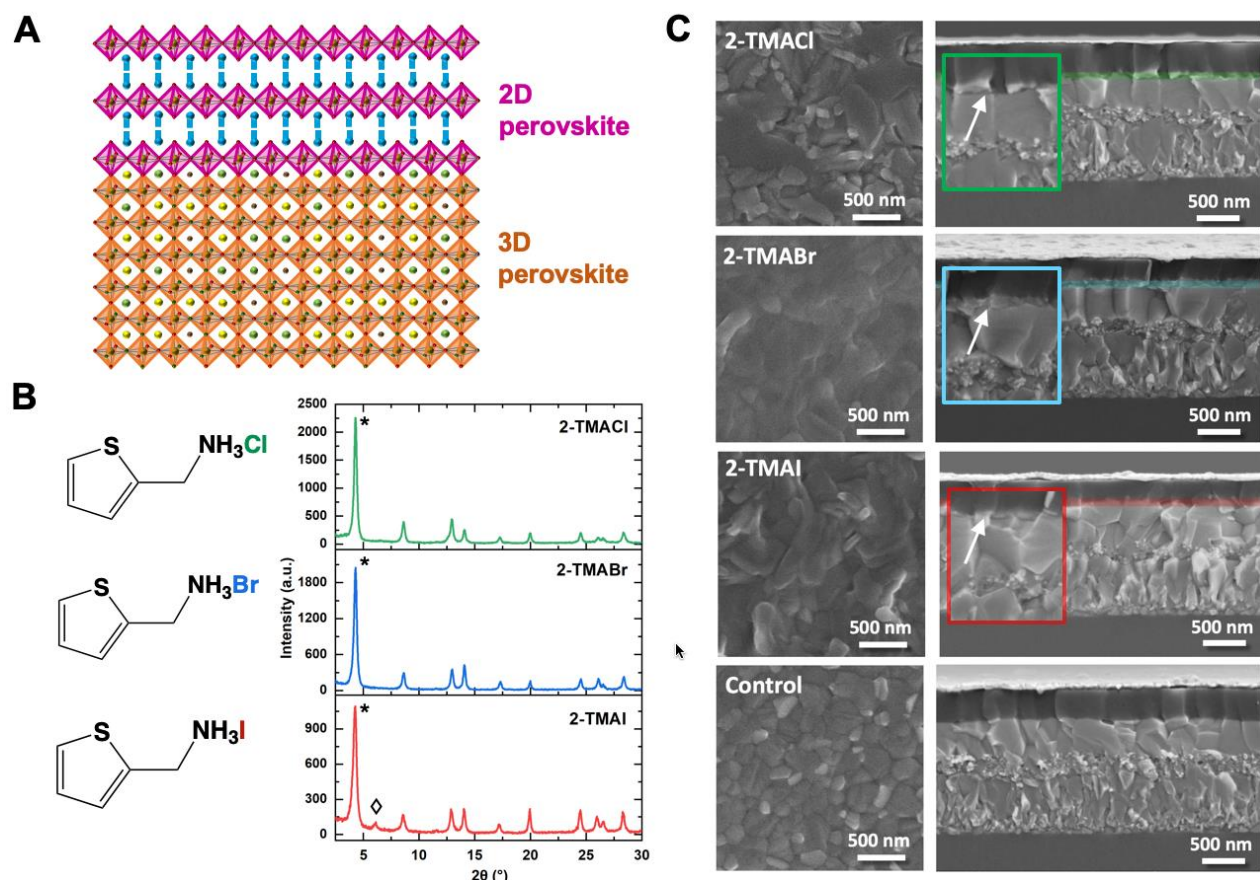


Figure 1. Structural and morphological characterization of 2D/3D perovskite films

(A) Schematic illustration of the 2D/3D perovskite interface.

(B) Molecular structure (left) and X-ray diffraction (XRD) pattern at 2° incident angle of the 2D/3D film employing 2-TMAI, 2-TMABr, and 2-TMACl respectively (\diamond and * denote 2D perovskite phase with $n=1$ and $n=2$, respectively).

(C) Top view (left) and cross-section (right) micrographs of the 3D only device as control and the 2D/3D perovskite solar cells (PSCs) employing 2-TMAI, 2-TMABr, and 2-TMACl. Insets show the magnified cross-section micrographs on the 2D/3D interface.

Table 1. Photovoltaic parameters of the champion PSCs based on 3D perovskite and 2D/3D perovskite hybrids employing 2-TMAI, 2-TMABr and 2-TMACl tested under AM 1.5G illumination (100 mW cm^{-2}).

	V_{oc} (V)	J_{sc} (mA cm^{-2})	FF	PCE (%)
2-TMAI/3D	1.09	24.2	0.76	19.9
2-TMABr/3D	1.15	23.2	0.78	20.8
2-TMACl/3D	1.16	22.8	0.74	19.7
Control	1.09	24.2	0.79	20.7

The absorption spectra of the 2D/3D thin films are reported in Figure S2, while Figure S3 shows the PL spectra upon excitation from the front side of the film. Notably, in all cases, a clear peak at lower wavelength region is observed, confirming to the formation of a distinct 2D perovskite overlayer. 2-TMAI-based 2D/3D exhibits PL emission peak at 520 and 570 nm which corresponds to $n=1$ and $n=2$ phase of 2D perovskite, respectively. On the other hand, 2-TMABr and 2-TMACl-based 2D/3D only show an emission peak at low wavelength region

(~ 545 nm) which is associated to $n=2$ phase. More in details, in agreement with what we recently reported,⁹ the 2-TMAI-based 2D/3D shows a slightly reduced band gap with respect to the 2-TMABr and 2-TMACl, as revealed by the photoluminescence peak emission shift (of around 0.1eV) in Figure S3.

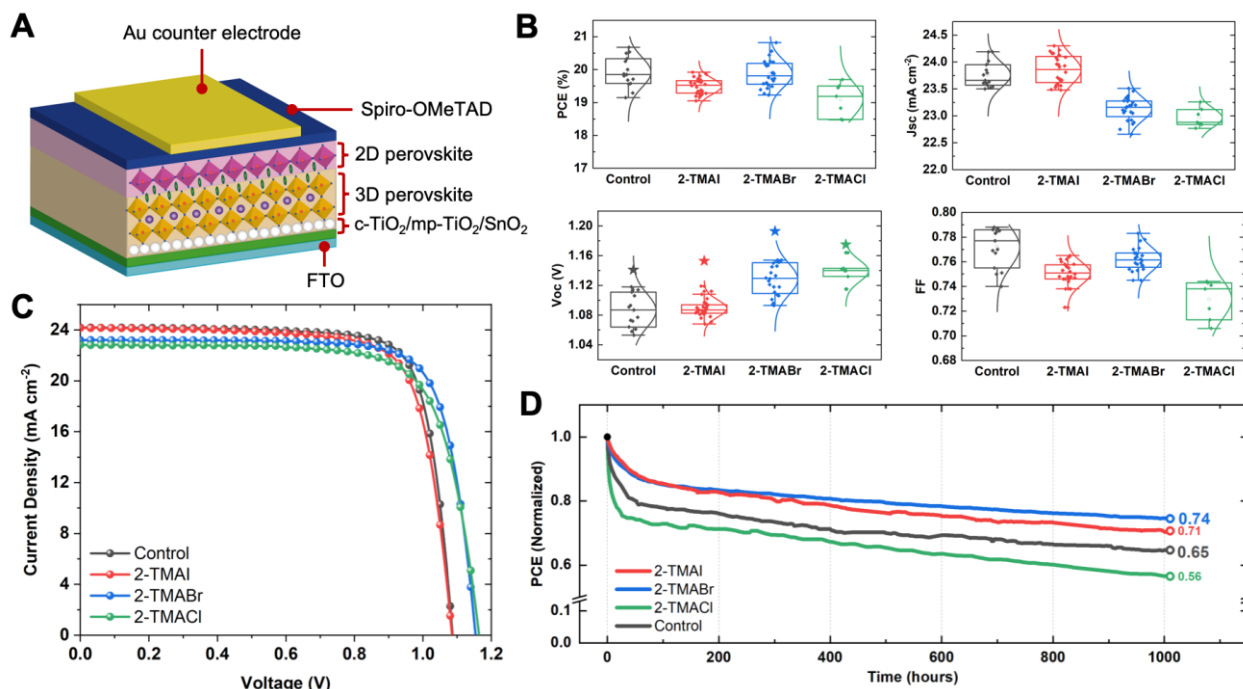


Figure 2. Photovoltaic performances of 2D/3D perovskite solar cells (PSCs)

(A) Schematic device structure of the 2D/3D PSCs.

(B) Statistics of the photovoltaics parameters of 3D PSCs as a control and 2D/3D PSCs based on 2-TMAI, 2-TMABr, 2-TMACl on over 70 devices. Note that the stars symbols in the V_{OC} subpanel represent the V_{OC} measured without using a mask.

(C) J-V curves of the champion cells of 3D and 2D/3D PSCs employing 2-TMAI, 2-TMABr, and 2-TMACl.

(D) Stability test under continuous 1 sun illumination for 1000 h in inert gas (Ar) atmosphere without any encapsulation. The stability data of 2-TMAI 2D/3D and control device were collected from the same experimental batch from our previous report⁹ for a fair comparison.

The photovoltaic (PV) response of the 2-TMAX based 2D/3D perovskite solar cells are shown in Figure 2 with the PV parameters for champion devices summarized in Table 1. With respect to the control, a clear increase in the V_{OC} is observed with the 2D perovskite layer, higher for 2-TMABr and 2-TMACl. It is important to note that the device V_{OC} reported here is underestimated due to the use of a small mask (0.16 cm^2) on a large pixel (0.54 cm^2). The reduction in V_{OC} values due to the mask effect could be calculated by the equation $\Delta V_{OC} = kT/q \ln(A_{aperture}/A_{device})$ where kT/q is the thermal voltage, $A_{aperture}$ is the mask aperture, and A_{device} is the pixel area.²⁷ Considering that the dark current of the pixel is not affected by the mask, this implies a ~ 3.4 -fold overestimation of the dark saturation current (J_0), which is equivalent to a voltage loss of 31 mV. By measuring without mask, the real maximum device voltage (shown by stars in Figure 2b) for the reference cell is 1.141 V, while for 2-TMAI, 2-TMABr and 2-TMACl, they are 1.153 V, 1.193V and 1.175V, respectively (see also Figure S4), among the highest values reported so far for $n-i-p$ devices with a mesoporous structure.

Importantly, the 2-TMABr shows a remarkable increase in V_{OC} , without compromising the fill factor (FF) which remains comparable to the control device, resulting in an overall increase in the device efficiency. On the other side, the 2-TMACl shows a reduction of the FF. The highest PV performance is therefore achieved with 2-TMABr-based 2D devices delivering a power conversion efficiency (PCE) of 20.82%. We note that this series of 2D perovskites, a slight

decrease in the short-circuit current (J_{sc}) is observed. This decrease might be related to the limitation in the charge transport induced by the presence of the bulky organic moieties. The long-term stability of the devices was monitored under continuous illumination of 1-sun intensity for 1000 hours in an argon atmosphere and is shown in Figure 2d. While the performance of the standard 3D device is reduced to 65% of its initial PCE, the 2D-functionalized solar cells shows a reduced loss in the PCE with the 2-TMABr/3D devices displaying the best stability retaining 75% of the initial PCE after 1000 hours. This confirms that the 2D surface functionalization has a crucial impact on the device lifetime with best performances reached with the 2-TMABr based 2D perovskite. 2D/3D perovskite devices are demonstrated to be highly sensitive to the nature of the organic cation which impact on the device V_{oc} and FF.

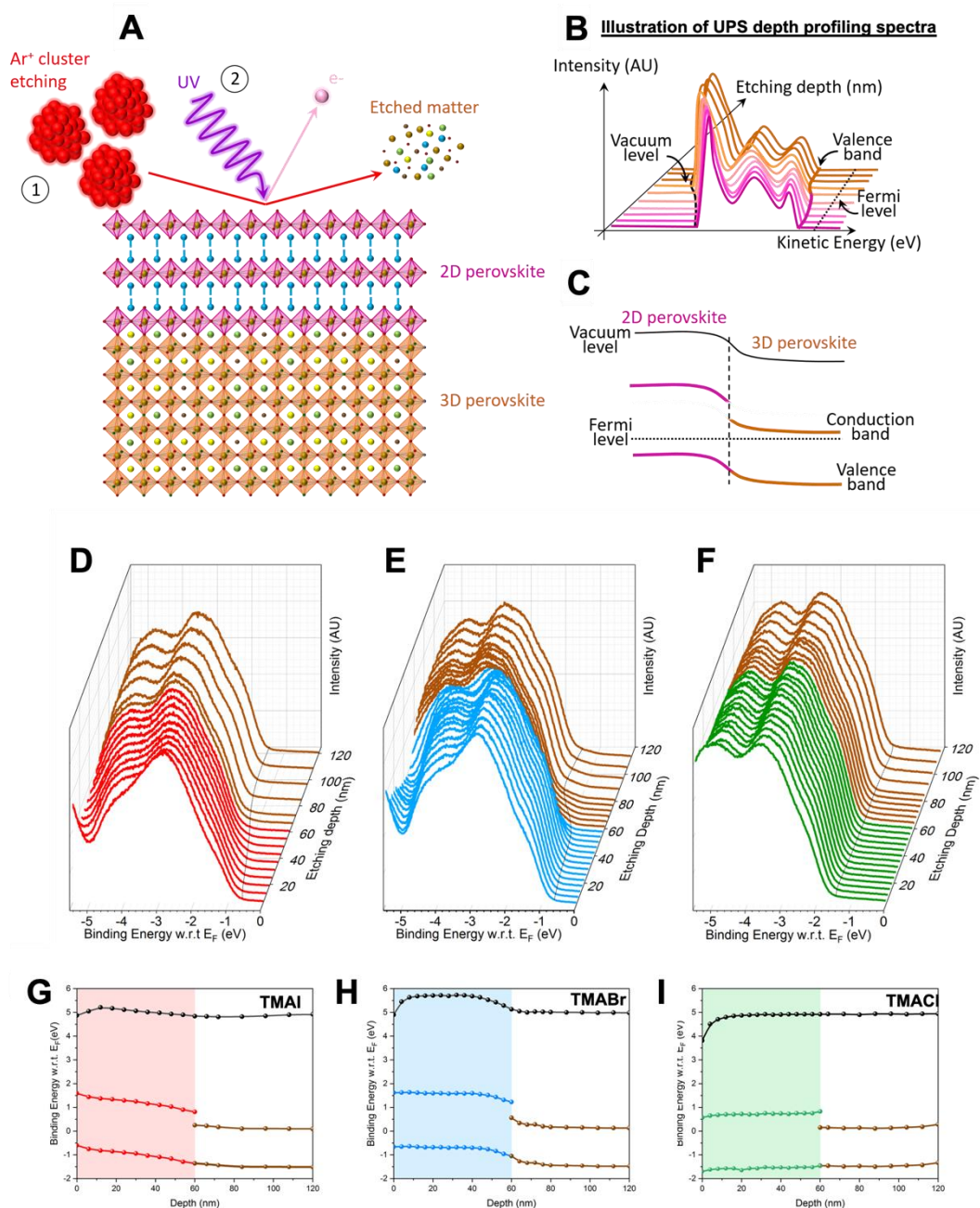


Figure 3. UPS depth measurement of 2D/3D perovskite interface.

- (A) Schematic representation of the UPS depth profiling technique which combines (1) etching by Ar ion clusters with (2) UPS measurements.
(B) Illustration of the evolution of the UPS spectra as a function of depth.
(C) The corresponding energy level diagram extracted from (B).
(D-I) Measured UPS spectra and corresponding energetic level diagrams of 2-TMAI (D,G), 2-TMABr (E,H), and 2-TMACl (F,I) with the 3D perovskite layer. Note: dashed line in UPS spectra is a guide to the eye.

We measure the vertical energy level landscape by an innovative UPS depth profiling technique.

To elucidate the link between material properties and device performances, it is necessary to directly probe the energetic alignment of the 2D/3D interfaces. Traditional methodology based on UPS measurements is only capable of probing the top 1-2 nm of the surface and will not provide insights regarding the buried 2D/3D interface. Recently, we developed a method termed ultra-violet photoemission spectroscopy (UPS) depth profiling technique, which allows probing the energetic landscape at the bulk of materials and across buried interfaces.²⁸ The principle of the technique is shown in Figure 3a and is based on the essentially damage-free etching enabled by Argon gas-cluster ion beams (1) in combination with UPS measurements (2) after each etching step. While this method has been previously applied solely to organic systems and organic/inorganic systems,²⁹⁻³¹ this is the first example of its application for the study of perovskite materials. Using this method, we are able to accurately measure the progression of the vacuum level and valence band positions as a function of film depth as depicted in the illustration in Figure 3b, providing for the first time an in-situ measurement of the interfacial energy levels alignment in a 2D/3D system (Figure 3c). The position of the conduction band is then estimated by adding the corresponding optical gap.

The UPS measurements reveal that the ionization potential (IP) of the 2D and 3D perovskites are all very similar (in the range 6.2-6.6 eV). This is in agreement with previous studies on BA_2PbI_4 (IP=6.5 eV) and BA_2PbBr_4 (IP=5.8eV),³² the IP values of which were found to be in good agreement with those of the corresponding 3D perovskites.^{33,34} The similarity of the IPs is also in agreement with the results of Zhang et al., that observe a change in IP of only 0.1 eV between the 3D and the 2D perovskites they investigated.³² The matching IPs explain why 2D perovskites can serve as capping layers for 3D perovskites in the *n-i-p* architecture in which they can permit the extraction of holes, whilst blocking electrons due to their higher lying conduction band.

While the ionization potentials of the materials are similar, UPS depth profiling of the three sets of 2D/3D samples reveals significant differences in their interfacial energetic alignment. Examining the band structure, it is clear that exchanging the halide on the bulky cations has important consequences for the evolution of the valence band levels: i) 2-TMABr and 2-TMAI show a shift in valence band compared to the 3D perovskite, indicating an effective energy level alignment to promote hole extraction, while 2-TMACl exhibited an opposite trend, with a slight uphill energy barrier (over the entire 2D layer). This results in the first two cases in the formation of a *p-n* junction which promotes charge extraction. Notably, this is consistent with the low FF observed in the 2-TMACl 2D/3D devices. ii) All the 2D/3D interfaces exhibit excellent electron blocking properties, with the energetic barrier being enhanced from 0.55 eV for 2-TMAI to 0.63 eV and 0.68 eV for 2-TMABr and 2-TMACl, respectively. The improvement in electron blocking suggests a more efficient reduction of minority carriers at the HTL interface of the device, in good agreement with corresponding enhancement in the open-circuit voltage observed from the photovoltaic results.

Notably, in all cases, the 3D perovskite is n-type, in agreement with the PbI_2 excess used in this case (see reference measurement on a 3D film in Figure S5).³⁴ Surprisingly, while the 2D layer formed by the 2-TMACl cation follows a similar character to that of the 3D perovskite, 2-TMABr and 2-TMAI denote a clear transition toward a *p*-type material. Such a transition is responsible for the formation of a *p-n* junction at the interface offering the possibility to improve the charge extraction and reduce interface recombination. This is particularly

evident for the 2-TMABr case as well as for the 2-TMAI case, while it is less manifested at the 2-TMACl based interface, possibly due to a less homogeneous 2D surface layer (see SEM top view in Figure 1c). As such, this proves that band bending happens at optimized 2D/3D perovskite interface, contributing in improving the device performance, as reported for other PV technologies.³⁵

the recombination mechanisms proposed is corroborated by drift-diffusion simulation

Similar formation of a *p-n* junction also occurs for other cations such as 2-thiopheneethylammonium iodide (2-TEAI) and 3-methylammonium iodide (3-TMAI) (Figure S6) which also show high photovoltaic performance.⁹

These results are also supported by numerical drift-diffusion device simulations, based on a well-established model,³⁶⁻⁴¹ which compare the effect of the additional 2D layer and the different energetic alignment scenarios based on the experimental results obtained for the reference 3D sample, 2-TMABr and 2-TMACl (Figure S7a-c). The effect of the enhanced electron blocking at the 2D/3D interface is evident when comparing the carrier densities in the proximity of the HTL interface (Figure S7d-f, dashed red circle). In the case of 2D/3D systems, the electron density at that interface is significantly reduced when compared to the reference 3D case. In excellent agreement with the experimental J-V results, when incorporating the 2-TMABr layer into the device structure, the simulated V_{OC} increases from $\sim 1.14V$ to $\sim 1.19V$ (Figure S7g). This increase can be attributed to the strong reduction of the electron density in the 2D in the proximity to the HTL which effectively limits the interfacial recombination losses (see Figure 3h).⁴² Overall, in case of the 2-TMABr cation, the band bending reduces the electron accumulation at the interface with the HTL, thereby reducing charge recombination while effectively driving holes to the HTM without inducing FF losses. Together these processes provide an effective mean to eliminate the severe non-radiative recombination loss at the HTM/perovskite interface.

To further corroborate these findings and to understand the physical processes governing these 2D/3D interfaces triggering the improvement in device V_{OC} , we measured the PL spectra as shown in Figure S8a-b and calculated the photoluminescence quantum yield (PLQY, Figure S8c). The PLQY values were then used to derive the Quasi Fermi Level Splitting (QFLS) in neat materials and complete solar cell devices as shown in Figure 4. This analysis allowed us to assess the relative contribution of bulk and interfacial recombination losses, but also the impact of the interfacial energy alignment.^{2, 39, 43} We note that the neat materials exhibit PLQYs over 1% (see Figure S8a,c), which is quite typical for mixed perovskites.

The results also highlight that the addition of a 2D layer improves the QFLS of the neat perovskite absorber (triangle in Figure 4a) indicating a trap passivating behavior and/or a reduction of minority charges at the defect-dense perovskite surface in the presence of the 2D layer.² More importantly, however, the PLQY of the 2-TMABr device approaches 2% which is far above average (see Figure S8b,c).³⁸ The deviation from the Shockley-Queisser radiative limit V_{OC} is due to mainly two factors. The first one is the non-radiative recombination in the perovskite absorber. As observed from the PLQY of the neat materials, the QFLS is already limited to roughly 1.25 eV, indicating a certain degree of recombination limiting the potential V_{OC} . The second limiting factor is interface recombination between the perovskite and the transport layers. Usually, the latter is strongly limiting the V_{OC} of Pb-based perovskite cells. Notably, in our 2D/3D system, since the QFLS of the neat materials matches with good degree to the V_{OC} of the complete device, the main voltage loss is only due to non-radiative recombination in the perovskite absorber layer, while interface recombination is essentially absent.

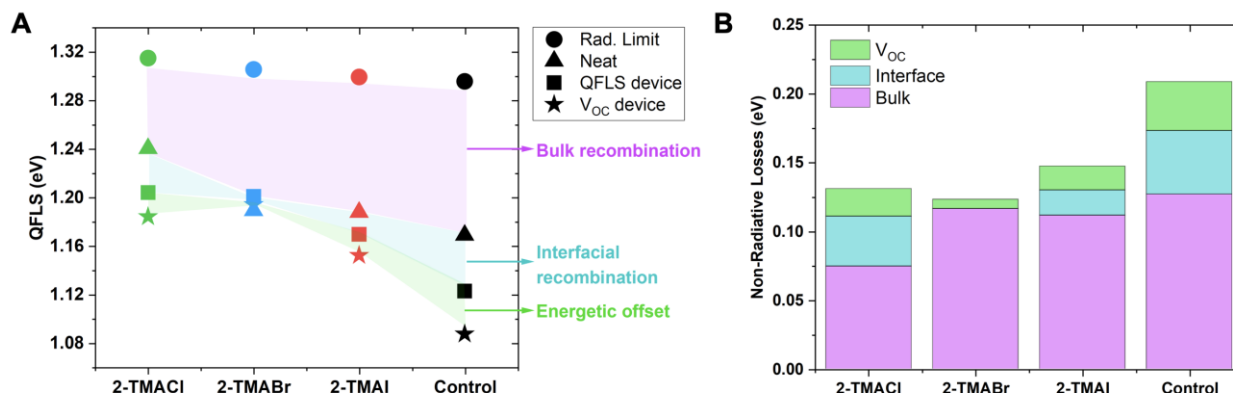


Figure 4. Calculated QFLS and calculated energy losses due to non-radiative recombination.

(A) QFLS calculated from the PLQY for the neat material and the full device for the different samples investigated in the study. Moreover, the Shockley-Queisser radiative limit and the experimental V_{OC} are plotted for each sample.

(B) Different type of energy losses calculated from (A) in order to compare the contribution of the different recombination processes for each system.

Figure 4 further shows that the trend in the non-radiative recombination losses in the devices as determined from the PLQY (squares in Figure 4) follows the trend observed in the J-V measurements. Interestingly, when the QFLS of the device is compared to the QFLS of the neat material, we found that all devices that employ the 2D layer display smaller energy losses due to less interfacial recombination losses compared to the reference cell. This confirms a key conclusion from the UPS measurements and the numerical simulations, which is that the 2D layer effectively reduces the density of minority carriers at the HTL interface. Importantly, the device based on 2-TMABr as cation exhibits an equal QFLS in the neat material and in the complete device, which is also approximately equal to the device V_{OC} (stars in Figure 4). This highlights the presence of a lossless perovskite/HTL interface and that the 2-TMABr/3D layer enables to reach the QFLS-potential of the neat perovskite layer.² These results are in accordance to the UPS depth profiling and simulations data.

we provide the exact knowledge on the interface energetics
it forms a p - n junction able of reducing the electron density at the hole
transport layer interface and ultimately suppressing interfacial recombination

However, in the case of the reference device and to a lesser extend in the devices with the other 2D layers, the internal QFLS is considerably higher than the external V_{OC} . As recently discussed, this effect can be explained by an internal bending of the hole quasi Fermi level, which impacts primarily the device V_{OC} rather QFLS in the perovskite layer and suggesting an energy misalignment between the perovskite and the transport layer which represents an additional interfacial recombination loss that is not captured by measuring the PL emission from the cell.^{38, 39} Considering that the internal QFLS is significantly higher than the external V_{OC} in the reference device suggests an energy misalignment between the perovskite and the spiro-OMeTAD. Hence, the application of 2D layers might further reduce the detrimental effect of an energetic misalignment between the perovskite and the spiro-OMeTAD layer as it effectively blocks the minority carriers from reaching the spiro-OMeTAD layer. In fact, we found that 2-TMABr and the formation of the p - n junction, is most effective at suppressing all interfacial recombination losses where the V_{OC} is only limited by the radiative efficiency of the neat material.

In conclusion, we demonstrate, by combining a comprehensive analysis on device performances, device and interface QFLS and interface energetics, that even subtle changes in the composition of the 2D perovskite can lead to differences of the energetic alignment at the 2D/3D interface, with a direct impact on charge density distribution, interfacial recombination and ultimately device performance. Our work provides the first demonstration of an optimized 2-TMABr based 2D/3D perovskite solar cells with zero interfacial voltage losses, reaching the QFLS-potential of the neat perovskite absorber and thus nullifying the energy losses at the interfaces. UPS depth profiling is demonstrated to be a valuable method allowing the direct probe of the interfacial alignment and band bending. Overall, this knowledge is essential to drive interfacial chemistry and functionalization to guide a smart device optimization. Combining chemical manipulation of the 2D perovskite and deep understanding of the 2D/3D interface energetics and recombination processes, our results provide clear evidence that 2D/3D interface engineering with optimal energetics allows to nullify the non-radiative interfacial recombination of electron and holes, demonstrating a breakthrough in the path to further enhance perovskite solar cell performance.

EXPERIMENTAL PROCEDURES

Synthesis of thiophenemethylammonium halides

A concentrated aqueous solution of an acid HX (1.1 eq, where X:Cl, Br or I) was added drop by drop to 1.0 M ethanol solution of thiophenemethylamine (1.0 eq) at 0°C under stirring. The mixture was allowed to reach room temperature gradually and then it was poured into an excess of diethyl ether (Et₂O). The precipitate was separated and washed thoroughly with Et₂O. The salts were recrystallized from ethanol (EtOH) and Et₂O mixtures, resulting in crystalline solids of the salts.

Perovskite thin-film and solar cells devices fabrication

Fluorine-doped tin oxide (FTO) substrates (Nippon Sheet Glass) were patterned by chemical etching process using zinc powder and aqueous HCl solution (3.0 M) and cleaned with the detergent (Hellmanex), water, acetone, and isopropanol subsequently. On top of the cleaned substrates, a 30-nm thick of compact TiO₂ layer as electron transporting layer was spray-deposited from the titanium diisopropoxide bis(acetylacetonate) solution (Sigma-Aldrich) precursor diluted in isopropanol (1:15 by volume fraction) at 450 °C, followed by the deposition of a 100 nm thick mesoporous TiO₂ layer by spin-coating a diluted TiO₂ paste solution in ethanol (1:8 w/v) at 5000 rpm for 20 s and sintering at 500°C for 20 min. A 20 nm of tin oxide layer as a passivation layer was formed from the aqueous tin (IV) chloride solution (12 μL SnCl₄ for 1mL solution) by depositing the SnCl₄ precursor at 3000 rpm for 30 s, followed by annealing at 100°C for 10 min and 190°C for 60 min. UV-ozone treatment was carried out for 15 min before both SnO₂ layer deposition and perovskite layer deposition.

A triple-cation based 3D perovskite precursor solution (1.3 M) with the composition of [(FAPbI₃)_{0.87}(MAPbBr₃)_{0.13}]_{0.92}(CsPbI₃)_{0.08} was prepared by mixing the starting materials (FAI (GreatCellSolar), MABr (GreatCellSolar), CsI (ABCR), PbI₂ (TCI), and PbBr₂ (TCI)) in DMF and DMSO mixture with the volume ratio of 0.78:0.22. An excess of PbI₂ by 5% towards FAI was used in the precursor solution in order to control the growth of the 2D perovskite layer. The 3D perovskite layer was deposited by spin-coating the precursor solution at 2000 rpm for 12 s and 5000 rpm for 30 s. Chlorobenzene was poured on top of the spinning substrate 15 s prior to the end of the spin-coating process. The deposited 3D perovskite film was annealed at 100°C for 60 min. Then, the film was allowed to cool down to the room temperature and the corresponding thiophene methylammonium halide cations (60 mM in isopropanol) was deposited dynamically under 4000 rpm for 30 s. The film was then annealed at 100°C for 6 min on a hotplate. Spiro-OMeTAD (Merck) with a concentration of 60 mmol in 1 mL of chlorobenzene as hole-transporting material doped with 31.28 μL of 4-tert-butylpyridine (Sigma-Aldrich), 18.57 μL of Li-bis (trifluoromethanesulphonyl) imide (Aldrich) from the stock solution (196 mg in 379 μL acetonitrile), and 13.69 μL of FK 209 Co(III) TFSI (GreatCellSolar) from the stock solution (99 mg in 263 μL acetonitrile) was deposited by spin-coating at 4000

rpm for 30 s. Finally, a gold counter electrode (70 nm) was deposited by physical vapor deposition process under high vacuum.

Thin-films Characterizations

Photoluminescence

Steady-state photoluminescence spectra were recorded on a Fluorolog3-22 spectrofluorometer upon excitation at 450 nm. The emission was measured from both top and bottom surface of the film.

UV-Vis absorption

An ultraviolet, visible, near-infrared spectrophotometer (PerkinElmer Lambda 950s) was used to measure the absorption spectra of the perovskite thin-films.

X-ray diffraction (XRD)

XRD patterns were acquired by measuring the perovskite thin-films using Bruker D8 Advance diffractometer and non-monochromated Cu-radiation. For the 2D/3D perovskite thin films, measurements under grazing incident diffraction (GID) geometry were performed on Bruker D8 Discover diffractometer with non-monochromated Cu-radiation at the incident angle of 2° in order to obtain the XRD patterns on the surface of the films.

Scanning electron microscopy (SEM)

SEM micrographs (cross-section and surface) were recorded in the FEI Teneo scanning electron microscope using in-lens detector under the accelerating voltage of 3 kV and 5 kV.

Ultra-violet photoemission spectroscopy (UPS) depth profiling (DP)

The samples were transferred to an ultrahigh vacuum chamber (ESCALAB 250Xi), with a base pressure of 2×10^{-10} mbar, for UPS DP measurements. UPS measurements were performed using a double-differentially pumped He gas discharge lamp emitting He I radiation ($h\nu=21.22$ eV) with a pass energy of 2 eV and a bias of -5 V in order to ensure secondary electron onset detection. The UPS spectra are shown as a function of the binding energy with respect to the Fermi Energy. The energy edge of the valence band features is used to determine the valence band level position with respect to the Fermi level. The onset of the valence band was analysed using a linear presentation of the UPS spectra. The secondary electron onset was used to determine the vacuum level with respect to the Fermi level. The conduction bands were estimated using the optical gaps of the 2D and 3D materials. Cluster etching was performed using large Ar clusters generated by the MAGCIS Dual Beam Ion Source (Thermo Scientific) with an energy of 4000 eV.

Absolute Photoluminescence

Excitation for the PL measurements was performed with a 445 nm continuous wave laser (Insaneware) through an optical fibre into an integrating sphere. The intensity of the laser was adjusted to a 1 sun equivalent intensity by illuminating a 1 cm² size perovskite solar cell under short-circuit and matching the current density to the J_{sc} under the sun simulator (22.0 mA cm⁻² at 100 mW cm⁻², or 1.375×10^{21} photons m⁻² s⁻¹). A second optical fiber was used from the output of the integrating sphere to an Andor SR393i-B spectrometer equipped with a silicon charge-coupled device camera (DU420A-BR-DD, iDus). The system was calibrated by using a calibrated halogen lamp with specified spectral irradiance, which was shone into to integrating sphere. A spectral correction factor was established to match the spectral output of the detector to the calibrated spectral irradiance of the lamp. The spectral photon density was obtained from the corrected detector signal (spectral irradiance) by division through the photon energy (hf) and the photon numbers of the excitation and emission obtained from numerical integration using Matlab. In a last step, three fluorescent test samples with high specified PLQY ($\approx 70\%$) supplied from Hamamatsu Photonics were measured where the specified value could be accurately reproduced within a small relative error of less than 5%. All PL measurements were performed on complete cells, prepared fresh, and immediately encapsulated in a glovebox under N₂ atmosphere. The PL of the samples was readily recorded after mounting the sample and after an exposure of 1 s at each laser intensity subsequently, the incident laser was blocked by a shutter and the filter wheel position adjusted while the sample was kept in dark conditions avoiding any effects induced by constant illumination. The cell was illuminated through the glass/ITO side. It was noted that all absolute PL

measurements were performed on films with the same HTL, ETL, and perovskite thicknesses as used in the operational solar cells.

Photovoltaic characterization

The current density–voltage (J–V) curves were measured under 1 sun illumination (AM 1.5G) in the ambient atmosphere and temperature using xenon lamp solar simulator (450 W, Oriel, AAA class). The light intensity was calibrated to 1 sun by using a Si reference equipped with an IR-cutoff (KG5) filter (Oriel 91150V). The current responses were measured using a digital source meter (Keithley 2400) by applying an external voltage bias. A metal mask with aperture of 0.16 cm² was used during the measurement in order to determine the active area. The J-V curves were scanned with the rate of 50 mV/s. No pre-biasing was applied prior to the measurements. External quantum efficiency (EQE) measurement was carried out by using IQE200B (Oriel).

Resource availability

Lead contact

Further information and requests for resources should be directed to and will be fulfilled by the lead contact, Giulia Grancini (giulia.grancini@unipv.it).

Materials availability

All materials generated in this study are available from the lead contact without restriction.

SUPPLEMENTAL INFORMATION

Document S1. Quantification of the QFLS in partial cell stacks, [Figures S1 – S11](#), Tables S1 – S2

ACKNOWLEDGMENTS

We acknowledge the Swiss National Science Foundation (SNSF) funding through Synergia Grant EPISODE (Grant No. CRSII5_171000). This project has received funding from the European Research Council (ERC) under the European Union's Horizon 2020 research and innovation programme (ERC Grant Agreement n° 714067, ENERGYPAPS) and the Deutsche Forschungsgemeinschaft (DFG) within the framework of SPP 2196, project PERFECTPVs (project #424216076). G.G. acknowledges the “HY-NANO” project that has received funding from the European Research Council (ERC) Starting Grant 2018 under the European Union's Horizon 2020 research and innovation programme (Grant agreement No. 802862). MS acknowledges the DFG - project number 423749265 and 03EE1017C - SPP 2196 (SURPRISE and HIPSTER) for funding. The authors acknowledge the Swiss National Science Foundation (SNSF) funding through the Ambizione Energy project Hyper (Grant number PZENP2_173641). We acknowledge Dr. Pascal A. Schouwink for the assistance in grazing-incident angle XRD measurements. We acknowledge Prof. Raffaella Buonsanti for the use of Fluorog system.

AUTHOR CONTRIBUTIONS

G.G., A.A.S., and D.N. conceived the original idea of the work. N.D. designed the organic salts, A.A.S. fabricated the thin films and PSCs and characterised them, I.G.B. performed the initial 2D materials investigation and V.I.E.Q. performed the steady-state PL measurements, with and under the supervision of G.G.

DECLARATION OF INTERESTS

The authors declare no competing interests.

REFERENCE

1. Shao, S., and Loi, M. A. (2020). The Role of the Interfaces in Perovskite Solar Cells. *Advanced Materials Interfaces* 7, 1901469. [10.1002/admi.201901469](https://doi.org/10.1002/admi.201901469).

2. Stolterfoht, M., Grischek, M., Caprioglio, P., Wolff, C. M., Gutierrez-Partida, E., Peña-Camargo, F., Rothhardt, D., Zhang, S., Raoufi, M., Wolansky, J., et al. (2020). How To Quantify the Efficiency Potential of Neat Perovskite Films: Perovskite Semiconductors with an Implied Efficiency Exceeding 28%. *Adv. Mater.* **32**, 2000080. [10.1002/adma.202000080](https://doi.org/10.1002/adma.202000080).
3. Grancini, G., Roldán-Carmona, C., Zimmermann, I., Mosconi, E., Lee, X., Martineau, D., Nabey, S., Oswald, F., De Angelis, F., Graetzel, M., et al. (2017). One-Year Stable Perovskite Solar Cells by 2D/3D Interface Engineering. *Nat. Commun.* **8**, 15684. [10.1038/ncomms15684](https://doi.org/10.1038/ncomms15684).
4. Cho, K. T., Grancini, G., Lee, Y., Oveisi, E., Ryu, J., Almora, O., Tschumi, M., Schouwink, P. A., Seo, G., Heo, S., et al. (2018). Selective Growth of Layered Perovskites for Stable and Efficient Photovoltaics. *Energy Environ. Sci.* **11**, 952-959. [10.1039/c7ee03513f](https://doi.org/10.1039/c7ee03513f).
5. Cho, K. T., Zhang, Y., Orlandi, S., Cavazzini, M., Zimmermann, I., Lesch, A., Tabet, N., Pozzi, G., Grancini, G., and Nazeeruddin, M. K. (2018). Water-Repellent Low-Dimensional Fluorous Perovskite as Interfacial Coating for 20% Efficient Solar Cells. *Nano Lett.* **18**, 5467-5474. [10.1021/acs.nanolett.8b01863](https://doi.org/10.1021/acs.nanolett.8b01863).
6. García-Benito, I., Quarti, C., Quelo, V. I. E., Orlandi, S., Zimmermann, I., Cavazzini, M., Lesch, A., Marras, S., Beljonne, D., Pozzi, G., et al. (2018). Fashioning Fluorous Organic Spacers for Tunable and Stable Layered Hybrid Perovskites. *Chem. Mater.* **30**, 8211-8220. [10.1021/acs.chemmater.8b03377](https://doi.org/10.1021/acs.chemmater.8b03377).
7. Kim, H., Lee, S.-U., Lee, D. Y., Paik, M. J., Na, H., Lee, J., and Seok, S. I. (2019). Optimal Interfacial Engineering with Different Length of Alkylammonium Halide for Efficient and Stable Perovskite Solar Cells. *Adv. Energy Mater.* **9**, 1902740. [10.1002/aenm.201902740](https://doi.org/10.1002/aenm.201902740).
8. Yoo, J. J., Wieghold, S., Sponseller, M. C., Chua, M. R., Bertram, S. N., Hartono, N. T. P., Tresback, J. S., Hansen, E. C., Correa-Baena, J.-P., Bulović, V., et al. (2019). An interface stabilized perovskite solar cell with high stabilized efficiency and low voltage loss. *Energy Environ. Sci.* **12**, 2192-2199. [10.1039/C9EE00751B](https://doi.org/10.1039/C9EE00751B).
9. Sutanto, A. A., Drigo, N., Quelo, V. I. E., García-Benito, I., Kirmani, A. R., Richter, L. J., Schouwink, P. A., Cho, K. T., Paek, S., Nazeeruddin, M. K., et al. (2020). Dynamical Evolution of the 2D/3D Interface: A Hidden Driver Behind Perovskite Solar Cell Instability. *J. Mater. Chem. A* **8**, 2343-2348. [10.1039/C9TA12489F](https://doi.org/10.1039/C9TA12489F).
10. Liu, Y., Akin, S., Pan, L., Uchida, R., Arora, N., Milić, J. V., Hinderhofer, A., Schreiber, F., Uhl, A. R., Zakeeruddin, S. M., et al. (2019). Ultrahydrophobic 3D/2D fluoroarene bilayer-based water-resistant perovskite solar cells with efficiencies exceeding 22%. *Science Advances* **5**, eaaw2543. [10.1126/sciadv.aaw2543](https://doi.org/10.1126/sciadv.aaw2543).
11. Jung, E. H., Jeon, N. J., Park, E. Y., Moon, C. S., Shin, T. J., Yang, T.-Y., Noh, J. H., and Seo, J. (2019). Efficient, Stable and Scalable Perovskite Solar Cells Using Poly(3-hexylthiophene). *Nature* **567**, 511-515. [10.1038/s41586-019-1036-3](https://doi.org/10.1038/s41586-019-1036-3).
12. Yao, Q., Xue, Q., Li, Z., Zhang, K., Zhang, T., Li, N., Yang, S., Brabec, C. J., Yip, H.-L., and Cao, Y. (2020). Graded 2D/3D Perovskite Heterostructure for Efficient and Operationally Stable MA-Free Perovskite Solar Cells. *Adv. Mater.* **32**, 2000571. <https://doi.org/10.1002/adma.202000571>.
13. Min, H., Kim, M., Lee, S.-U., Kim, H., Kim, G., Choi, K., Lee, J. H., and Seok, S. I. (2019). Efficient, stable solar cells by using inherent bandgap of α -phase formamidinium lead iodide. *Science* **366**, 749-753. [10.1126/science.aay7044](https://doi.org/10.1126/science.aay7044).
14. Jeong, M., Choi, I. W., Go, E. M., Cho, Y., Kim, M., Lee, B., Jeong, S., Jo, Y., Choi, H. W., Lee, J., et al. (2020). Stable perovskite solar cells with efficiency exceeding 24.8% and 0.3-V voltage loss. *Science* **369**, 1615. [10.1126/science.abb7167](https://doi.org/10.1126/science.abb7167).
15. Bouduban, M. E. F., Quelo, V. I. E., Caselli, V. M., Cho, K. T., Kirmani, A. R., Paek, S., Roldán-Carmona, C., Richter, L. J., Moser, J. E., Savenije, T. J., et al. (2019). Crystal Orientation Drives the Interface Physics at Two/Three-Dimensional Hybrid Perovskites. *J. Phys. Chem. Lett.* **10**, 5713-5720. [10.1021/acs.jpcclett.9b02224](https://doi.org/10.1021/acs.jpcclett.9b02224).
16. Kim, J., Ho-Baillie, A., and Huang, S. (2019). Review of Novel Passivation Techniques for Efficient and Stable Perovskite Solar Cells. *Solar RRL* **3**, 1800302. [10.1002/solr.201800302](https://doi.org/10.1002/solr.201800302).
17. Ng, C. H., Hamada, K., Kapil, G., Kamarudin, M. A., Wang, Z., Iikubo, S., Shen, Q., Yoshino, K., Minemoto, T., and Hayase, S. (2020). Reducing trap density and carrier concentration by a Ge additive for an efficient quasi 2D/3D perovskite solar cell. *J. Mater. Chem. A*

- 8, 2962-2968.
10.1039/C9TA11989B.
18. Zuo, C., Scully, A. D., Tan, W. L., Zheng, F., Ghiggino, K. P., Vak, D., Weerasinghe, H., McNeill, C. R., Angmo, D., Chesman, A. S. R., et al. (2020). Crystallisation control of drop-cast quasi-2D/3D perovskite layers for efficient solar cells. *Communications Materials* **1**, 33. 10.1038/s43246-020-0036-z.
19. Mahmud, M. A., Duong, T., Yin, Y., Pham, H. T., Walter, D., Peng, J., Wu, Y., Li, L., Shen, H., Wu, N., et al. (2020). Double-Sided Surface Passivation of 3D Perovskite Film for High-Efficiency Mixed-Dimensional Perovskite Solar Cells. *Adv. Funct. Mater.* **30**, 1907962. <https://doi.org/10.1002/advf.201907962>.
20. Jang, Y.-W., Lee, S., Yeom, K. M., Jeong, K., Choi, K., Choi, M., and Noh, J. H. (2021). Intact 2D/3D halide junction perovskite solar cells via solid-phase in-plane growth. *Nat. Energy* **6**, 63-71. 10.1038/s41560-020-00749-7.
21. Luo, D., Su, R., Zhang, W., Gong, Q., and Zhu, R. (2020). Minimizing non-radiative recombination losses in perovskite solar cells. *Nat. Rev. Mater.* **5**, 44-60. 10.1038/s41578-019-0151-y.
22. Gutierrez-Partida, E., Hempel, H., Caicedo-Dávila, S., Raoufi, M., Peña-Camargo, F., Grischek, M., Gunder, R., Diekmann, J., Caprioglio, P., Brinkmann, K. O., et al. (2021). Large-Grain Double Cation Perovskites with 18 μ s Lifetime and High Luminescence Yield for Efficient Inverted Perovskite Solar Cells. *ACS Energy Lett.* **6**, 1045-1054. 10.1021/acsenergylett.0c02642.
23. Liu, Z., Krückemeier, L., Krogmeier, B., Klingebiel, B., Márquez, J. A., Levchenko, S., Öz, S., Mathur, S., Rau, U., Unold, T., et al. (2019). Open-Circuit Voltages Exceeding 1.26 V in Planar Methylammonium Lead Iodide Perovskite Solar Cells. *ACS Energy Lett.* **4**, 110-117. 10.1021/acsenergylett.8b01906.
24. deQuillettes, D. W., Koch, S., Burke, S., Paranj, R. K., Shropshire, A. J., Ziffer, M. E., and Ginger, D. S. (2016). Photoluminescence Lifetimes Exceeding 8 μ s and Quantum Yields Exceeding 30% in Hybrid Perovskite Thin Films by Ligand Passivation. *ACS Energy Lett.* **1**, 438-444. 10.1021/acsenergylett.6b00236.
25. Abdi-Jalebi, M., Andaji-Garmaroudi, Z., Cacovich, S., Stavrakas, C., Philippe, B., Richter, J. M., Alsari, M., Booker, E. P., Hutter, E. M., Pearson, A. J., et al. (2018). Maximizing and stabilizing luminescence from halide perovskites with potassium passivation. *Nature* **555**, 497-501. 10.1038/nature25989.
26. Sutanto, A. A., Szostak, R., Drigo, N., Queloz, V. I. E., Marchezi, P. E., Germino, J. C., Tolentino, H. C. N., Nazeeruddin, M. K., Nogueira, A. F., and Grancini, G. (2020). In Situ Analysis Reveals the Role of 2D Perovskite in Preventing Thermal-Induced Degradation in 2D/3D Perovskite Interfaces. *Nano Lett.* **20**, 3992-3998. 10.1021/acsnanolett.0c01271.
27. Kiermasch, D., Gil-Escrig, L., Bolink, H. J., and Tvingstedt, K. (2019). Effects of Masking on Open-Circuit Voltage and Fill Factor in Solar Cells. *Joule* **3**, 16-26. <https://doi.org/10.1016/j.joule.2018.10.016>.
28. Lami, V., Weu, A., Zhang, J., Chen, Y., Fei, Z., Heeney, M., Friend, R. H., and Vaynzof, Y. (2019). Visualizing the Vertical Energetic Landscape in Organic Photovoltaics. *Joule* **3**, 2513-2534. <https://doi.org/10.1016/j.joule.2019.06.018>.
29. Lami, V., Hofstetter, Y. J., Butscher, J. F., and Vaynzof, Y. Energy Level Alignment in Ternary Organic Solar Cells. *Advanced Electronic Materials* **n/a**, 2000213. 10.1002/aeml.202000213.
30. Zhang, J., Futscher, M. H., Lami, V., Kosasih, F. U., Cho, C., Gu, Q., Sadhanala, A., Pearson, A. J., Kan, B., Divitini, G., et al. (2019). Sequentially Deposited versus Conventional Nonfullerene Organic Solar Cells: Interfacial Trap States, Vertical Stratification, and Exciton Dissociation. *Adv. Energy Mater.* **9**, 1902145. 10.1002/aeml.201902145.
31. Wittmann, A., Schweicher, G., Broch, K., Novak, J., Lami, V., Cornil, D., McNellis, E. R., Zadvorna, O., Venkateshvaran, D., Takimiya, K., et al. (2020). Tuning Spin Current Injection at Ferromagnet-Nonmagnet Interfaces by Molecular Design. *Phys. Rev. Lett.* **124**, 027204. 10.1103/PhysRevLett.124.027204.
32. Zhang, T., Long, M., Qin, M., Lu, X., Chen, S., Xie, F., Gong, L., Chen, J., Chu, M., Miao, Q., et al. (2018). Stable and Efficient 3D-2D Perovskite-Perovskite Planar Heterojunction Solar Cell without Organic Hole Transport Layer. *Joule* **2**, 2706-2721. <https://doi.org/10.1016/j.joule.2018.09.022>.
33. Falk, L. M., Goetz, K. P., Lami, V., An, Q., Fassel, P., Herkel, J., Thome, F., Taylor, A. D., Paulus, F., and Vaynzof, Y. (2020). Effect of Precursor Stoichiometry on the Performance and

- Stability of MAPbBr₃ Photovoltaic Devices. *Energy Technology* **8**, 1900737. 10.1002/ente.201900737.
34. Fassel, P., Lami, V., Bausch, A., Wang, Z., Klug, M. T., Snaith, H. J., and Vaynzof, Y. (2018). Fractional deviations in precursor stoichiometry dictate the properties, performance and stability of perovskite photovoltaic devices. *Energy Environ. Sci.* **11**, 3380-3391. 10.1039/C8EE01136B.
35. Cui, P., Wei, D., Ji, J., Huang, H., Jia, E., Dou, S., Wang, T., Wang, W., and Li, M. (2019). Planar p-n homojunction perovskite solar cells with efficiency exceeding 21.3%. *Nat. Energy*. **4**, 150-159. 10.1038/s41560-018-0324-8.
36. Diekmann, J., Caprioglio, P., Rothhardt, D., Arvind, M., Unold, T., Kirchartz, T., Neher, D., and Stolterfoht, M. Pathways towards 30% efficient perovskite solar cells 2019. <https://arxiv.org/abs/1910.07422>.
37. Caprioglio, P., Wolff, C. M., Sandberg, O. J., Armin, A., Rech, B., Albrecht, S., Neher, D., and Stolterfoht, M. (2020). On the Origin of the Ideality Factor in Perovskite Solar Cells. *Adv. Energy Mater.* **10**, 2000502. 10.1002/aenm.202000502.
38. Stolterfoht, M., Caprioglio, P., Wolff, C. M., Márquez, J. A., Nordmann, J., Zhang, S., Rothhardt, D., Hörmann, U., Amir, Y., Redinger, A., et al. (2019). The impact of energy alignment and interfacial recombination on the internal and external open-circuit voltage of perovskite solar cells. *Energy Environ. Sci.* **12**, 2778-2788. 10.1039/C9EE02020A.
39. Caprioglio, P., Stolterfoht, M., Wolff, C. M., Unold, T., Rech, B., Albrecht, S., and Neher, D. (2019). On the Relation between the Open-Circuit Voltage and Quasi-Fermi Level Splitting in Efficient Perovskite Solar Cells. *Adv. Energy Mater.* **9**, 1901631. 10.1002/aenm.201901631.
40. Stolterfoht, M., Le Corre, V. M., Feuerstein, M., Caprioglio, P., Koster, L. J. A., and Neher, D. (2019). Voltage-Dependent Photoluminescence and How It Correlates with the Fill Factor and Open-Circuit Voltage in Perovskite Solar Cells. *ACS Energy Lett.* **4**, 2887-2892. 10.1021/acscenergylett.9b02262.
41. Stolterfoht, M., Wolff, C. M., Márquez, J. A., Zhang, S., Hages, C. J., Rothhardt, D., Albrecht, S., Burn, P. L., Meredith, P., Unold, T., et al. (2018). Visualization and Suppression of Interfacial Recombination for High-Efficiency Large-Area pin Perovskite Solar Cells. *Nat. Energy*. **3**, 847-854. 10.1038/s41560-018-0219-8.
42. Wolff, C. M., Caprioglio, P., Stolterfoht, M., and Neher, D. (2019). Nonradiative Recombination in Perovskite Solar Cells: The Role of Interfaces. *Adv. Mater.* **31**, 1902762. 10.1002/adma.201902762.
43. Wang, Q., Zu, F., Caprioglio, P., Wolff, C. M., Stolterfoht, M., Li, M., Turren-Cruz, S.-H., Koch, N., Neher, D., and Abate, A. (2020). Large Conduction Band Energy Offset Is Critical for High Fill Factors in Inorganic Perovskite Solar Cells. *ACS Energy Lett.* **5**, 2343-2348. 10.1021/acscenergylett.0c00980.